Colloids and Surfaces B: Biointerfaces
Volume 237, May 2024, 113864
https://doi.org/10.1016/j.colsurfb.2024.113864

Interfacial blending in co-axially electrospun polymer core-shell fibers and their interaction with cells via focal adhesion point analysis

Martyna Polak[1], Daniel P. Ura[1], Krzysztof Berniak[1], Piotr K. Szewczyk[1], Mateusz M. Marzec[2], Urszula Stachewicz[1,]*

[1]Faculty of Metals Engineering and Industrial Computer Science, [2]Academic Centre for Materials and Nanotechnology, AGH University of Krakow, Al. A. Mickiewicza 30, Kraków 30-059, Poland

*E-mail: ustachew@agh.edu.pl

KEYWORDS

Osteoblasts, cell-material interaction, focal adhesion, co-axial electrospinning, blend polymers, core-shell fibers

Short Statistical Summary

Number of words: 8017

Number of tables: 2

Number of figures: 6

ABSTRACT

Electrospun polymer scaffolds have gained prominence in biomedical applications, including tissue engineering, drug delivery, and wound dressings, due to their customizable properties. As the interplay between cells and materials assumes fundamental significance in biomaterials research, understanding the relationship between fiber properties and cell behaviour is imperative. Nevertheless, altering fiber properties introduces complexity by intertwining mechanical and surface chemistry effects, challenging the differentiation of their individual impacts on cell behaviour. Core-shell fibers present an appealing solution, enabling the control of mechanical properties of scaffolds, flexibility in material and drug selection, efficient encapsulation, strong protection of bioactive drugs against harsh environments, and controlled, prolonged drug release. This study addresses a key challenge in core-shell fiber design related to the blending effect between core and shell polymers. Two types of fibers, PMMA and core-shell PC-PMMA, were electrospun, and thorough analyses confirmed the desired core-shell structure in PC-PMMA fibers. Surface chemistry analysis revealed PC diffusion to the PMMA shell of the core-shell fiber during electrospinning, subsequently prompting an investigation of the fiber's surface potential. Conducting cellular studies on osteoblasts by super-resolution confocal microscopy provided insights into the direct influence of interfacial polymer blending and, consequently, altered fiber surface and mechanical properties on cell focal adhesion points, bridging the gap between material attributes and cell responses in core-shell fibers.

1. Introduction

Electrospun polymer scaffolds are widely used in biomedical applications such as tissue engineering, drug delivery systems, or wound dressings due to the tunability of their properties[1–5]. As the interaction between cells and materials represents a crucial and fundamental area of study in biomaterials research, the relationship between fiber properties and cell behaviour needs to be investigated[6–8]. Electrospinning, due to a wide variety of changeable processing parameters, allows the manipulation of the surface, mechanical or geometrical properties of fibers directly affecting the proliferation, differentiation, or attachment of cells[9–11]. Electrospun scaffolds are designed to mimic the extracellular matrix (ECM), which is a network consisting of minerals, proteins, and enzymes that provide structural and biochemical support for cells[12,13].

One drawback of modifying fiber's mechanics using techniques like photopolymerization and blending is the introduction of interdependence between mechanics and surface chemistry, making it challenging to distinguish their individual effects on cell behaviour. For example, polymer blends can alter the surface roughness and hydrophilicity of fibers, consequently affecting cell attachment and their mechanical interactions within the environment[14,15]. However, blend electrospun fibers are an attractive method of drug encapsulation for drug delivery systems and tissue engineering[15–19]. In contrast, core-shell fibers provide an appealing alternative, allowing independent control of mechanical properties without influencing surface chemistry and scaffold geometry[20,21]. Numerous drug delivery methods have been thoroughly explored, encompassing polymer micelles, liposomes, gels, complexes, and co-axially electrospun fibers[22]. Among these, core-shell fibers offer distinct advantages such as flexibility in material and drug selection, efficient encapsulation, strong protection of bioactive drugs against harsh environments, cost-effectiveness, ease of operation, and controlled, prolonged drug release. This makes core-shell

fibers an attractive appealing option for drug delivery[23]. Moreover, many studies show the successful incorporation of bioactive substances in the shell of fibers to increase their effects due to exposure at the surface of fibers and induce cellular responses[24–26]. In this study, we introduce a challenge in core-shell fibers design related to the occurrence of a blending effect between core and shell polymers. While highly porous scaffolds made of electrospun fibers can successfully emulate significant characteristics of the extracellular matrix in tissue engineering, they face a limitation in their inability to safely incorporate and release biocompounds such as drugs and growth factors in a controlled manner[27]. Here, the interfacial blending effect in core-shell fibers, such as drug delivery systems, should be considered.

In our research, we produced two types of fibers, PMMA (polymethyl methacrylate) and core-shell PC-PMMA (polycarbonate – polymethyl methacrylate), by electrospinning. We analyzed the morphology of the fibers, bulk and surface chemistry, thermal properties, and finally, mechanical properties, proving the formation of the correct core-shell structure in PC-PMMA fibers. The surface chemistry, crucial from the point of view of interactions with cells, showed the occurrence of PC in the surface of PC-PMMA fibers, which consequently led us to the analysis of the surface potential of the fibers using Kelvin probe force microscopy (KPFM). Further, the surface chemistry analysis helped to investigate PC diffusion to the surface of core-shell fibers that occurred during the co-axial electrospinning. As the next step, we performed a series of cellular studies on osteoblasts, including unique super-resolution confocal microscopy, which allowed us to investigate the direct effect of changes in fiber properties on cell adhesion points[28]. How cells adhere to substrate materials significantly impacts cell function and tissue development. Cell adhesion sets off signaling cascades that possess the capacity to govern a range of processes, encompassing embryogenesis, tissue differentiation, and cell migration. While focal adhesion size

and assembly can be considered a critical cue for the correlation between cellular behaviour, functions, and substrate properties, we investigated this relation[29,30].

2. Materials and methods

2.1. Materials

Polycarbonate granulate (PC, Makrolon 3108, Goodfellow GmbH, Germany) was dissolved in a mixture of N, N-dimethylformamide (DMF, Sigma Aldrich, UK) and N, N-dimethyloacetamide (DMAC, Thermo Fisher Scientific, USA) at 1:1 wt. ratio in the concentration of 24 wt. %. The second solution was produced by dissolving 14 wt % of polymethyl methacrylate (PMMA, 350 000 g mol^{-1}, Sigma Aldrich, UK) in DMF. Solutions were stirred at 1000 rpm for 3 h on a hot plate set at 60 °C (IKA RCT basic, Staufen, Germany).

2.2. Electrospinning

Both types of fibers were electrospun (EC-DIG apparatus with climate control, IME Technologies, the Netherlands) at 25 °C and relative humidity of 40 %. Fabrication of PMMA fibers required using a stainless-steel nozzle (0.51 mm inner (ID) and 0.82 mm outer diameter (OD), 21G x 1 ½"). PC-PMMA core-shell fibers were produced using a coaxial nozzle (IME Technologies, the Netherlands) with an ID of 0.4 mm and a shell nozzle diameter of 1.2 mm. For PMMA fibers the distance between the nozzle and the collector was 15 cm, and the voltage applied to the nozzle of 14 kV, while for PC-PMMA core-shell fibers it was 25 cm, and 13 kV, respectively. The flow rate for electrospinning PMMA fibers was 4 mLh^{-1}, and for PC-PMMA core-shell fibers 2.8 $mL^{-1}h$ of PC solution and 3.2 mLh^{-1} of PMMA solution.

2.3. Scanning electron microscopy (SEM)

Prior to SEM imaging, samples were coated with an 8 nm Au layer using rotary-pumped sputter coating (Q150RS, Quorum Technologies, UK). Then, samples were imaged with the SEM (Merlin

Gemini II, Zeiss, Germany) using a SE detector, applying a current of 100 – 150 pA, a voltage of 3 kV, and a working distance of 3 – 9 mm. Diameters of the fibers D_f were analyzed from SEM images using ImageJ software (ImageJ 2.1.0, USA), and the average value was calculated from 100 measurements taken from SEM micrographs and presented in Figure 1 using Gaussian fit. For cross-section investigation fibers were immersed in liquid N_2 for 5 min and cut using a scalpel.

2.4. Contact angle measurement

Deionized water (Spring 5UV purification system, Hydrolab, Poland) droplets of 3 µL volume were deposited onto the surface of electrospun PMMA and PC-PMMA membranes. Images were taken using the camera with the macro lens (EOS 700D camera with EF-S 60 mm f/2.8 Macro USM, Canon, Japan) in the first 3 s from droplet deposition. Contact angles were measured using ImageJ software (ImageJ 2.1.0, USA). The average water contact angle was obtained from measurements of ten droplets per sample.

2.5. Bulk chemistry and structure analysis

The bulk chemistry of PMMA powder, PC granules, PMMA, and PC-PMMA fibers was investigated with Fourier transform infrared spectroscopy (FTIR, Nicolet iS5, Thermo Fisher, USA). The samples were scanned in a range of 400 to 4000 cm^{-1} in a total scan number of 64.

Differential scanning calorimetry (DSC) carried out using DSC 3 (Mettler Toledo, Switzerland) allowed the analysis of thermal properties of PMMA powder, PC granules, and both PMMA and PC-PMMA electrospun fibers. The results present the average values taken from the three independent measurements of each sample. Samples were heated at a rate of 10 $Kmin^{-1}$ from -20 °C to 300 °C.

2.6. Mechanical tests

Fibrous mats were laser-cut into rectangular samples with a size of 130×70 mm, which were later tested using a tensile machine (20 N cell, Kammrath & Weiss, Germany) at T=24 °C and RH=40%, with an extension rate 25 μms^{-1}. The stress was determined by dividing the force measured by the machine by the initial cross-section of the electrospun mats. The thickness of the samples was measured using a light microscope (Axio Imager M1m, ZEISS, Germany) in the z-direction at 5 different points on each sample. To obtain the average values for toughness (W), maximum stress (R_m), elongation at maximum stress (ε_{max}), and elongation at failure (ε_f), five separate measurements were taken and then calculated using the Integrate function in the OriginPro software (ver. 2022 9.9 USA).

For tensile tests of single and two fibers, fibers were deposited directly onto the paper frames, with an inside hole size of 1×2 mm, during the electrospinning. The presence of fibers on the frames and their alignment along the stretching direction was verified with a light microscope (Primo Star 1, ZEISS, Germany). Analogical characteristic values were calculated as it was done for fibrous mats. Additionally, using the slope value of linear fitting in the OriginPro software (ver. 2022 9.9 USA), it was possible to calculate the value of Young's Modulus. The diameter of fibers required for calculations was determined as the average diameter measured from SEM images as mentioned above.

2.7. Surface properties investigation

The surface chemistry analysis of fibers deposited onto silicon wafers was conducted using the Angle-Resolved XPS (ARXPS PHI VersaProbeII Scanning XPS) system. Monochromatic Al Kα (1486.6 eV) X-rays were used, focused to a 100 μm spot. To achieve high energy resolution spectra for the C 1s and O 1s regions, the photoelectron take-off angles were varied at 10º and 90º. The analyzer's pass energy was set to 46.95 eV with a 0.1 eV step. Dual beam charge compensation

was employed using 7 eV Ar+ ions and 1 eV electrons, irrespective of the sample conductivity to maintain a constant sample surface potential. All XPS spectra were charge referenced to the unfunctionalized, saturated carbon (C–C) C1s peak at 285.0 eV. The operating pressure in the analytical chamber was kept below 2×10^{-9} mbar. For data analysis, spectra deconvolution was performed using PHI MultiPak software (v.9.9.3), and the Shirley method was used for spectrum background subtraction.

Kelvin probe force microscopy (KPFM) measurements were conducted using the CoreAFM system (Nanosurf, Switzerland). For KPFM measurements, conductive HQ:NSC18/Pt tips (MikroMasch, Bulgaria), with a force constant of 2.8 Nm^{-1} and a resonance frequency of 75 kHz were utilized. During the measurements, topography data was obtained simultaneously with KPFM, and scanning areas of 15 × 15 μm^2 and 50 × 50 μm^2 were used depending on the specific measurement. KPFM data was generated by averaging scan lines taken from the apex of 7 different fibers measured on 4 separate scan regions. To serve as a control measurement of the KPFM signal, measurements from the ITO layer of the glass were taken alongside fibers. All measurements were performed in a single session to ensure consistent environmental conditions of RH at 50–65% and 23 °C. The values for ITO represent an average of 10 separate lines on each of the 4 scans. Data was processed using Gwyddion (v2.56, gwyddion.net) and OriginPro (v9.7.0.188, OriginLab Corporation, USA) software.

2.8. Cell culture study

2.8.1. Cell proliferation

The cell culture study was performed using human osteoblast-like cells (MG-63) (Sigma Aldrich, UK). Before cell seeding, scaffolds were cut into 15 mm diameter circles, placed in 24-well plates, and sterilized with UV light for 30 min. Tissue culture polystyrene (TCPS) was used

as a control. The cell density of 2×10^4 cells per 1 ml in culture media was used for the proliferation assay. Incubation was provided at 37 ºC and RH of 95 % in a 5 % CO_2 atmosphere in the incubator (Memmert GmbH Co.KG, INC 108med, Schwabach, Germany). The cellular medium consisted of Dulbecco's modified Eagle Medium (DMEM with 4.5 g/LD – glucose, Biological Industries, Israel), supplemented with 10 % of fetal bovine serum (FBS, Biological Industries, Israel), 2 % of antibiotics (penicillin−streptomycin, Biological Industries, Israel), 1 % of L-glutamine solution (Biological Industries, Israel), and 1 % of amino acids (mem nonessential amino acid solution 100×, Sigma-Aldrich, USA).

Proliferation tests were done using the CellTiter-BlueR©Assay (GloMax Discover plate Reader, Promega, USA). Cell viability was evaluated after 1, 3, and 7 days of incubation. After each time point, the media was replaced with 1 ml of media containing 20 % of CellTiter-BlueR© reagent (Promega, USA), and incubated for 4 h at 37 ºC. From each well, 100 µm of reagent was transferred to a 96-well plate in triplicates, and fluorescence was read at 560/590 nm using the microplate reader GloMaxR©DiscoverSystem (Promega, USA). For the cell culture study, tests were conducted on two repetitions for each type of fibers and control. The statistical analysis was performed in OriginPro (ver. 2022 9.9 USA) using a one-way Analysis of variance (ANOVA) and Tukey's *post hoc* test. Differences were considered statistically significant when $p < 0.05$.

2.8.2. Confocal microscopy imaging: nuclei, actin, and focal adhesion staining

For proliferation study, cells were seeded on samples as well as on glass and cultured for 1, 3, and 7 days. In the case of focal adhesion investigation, cells were seeded and cultured on samples for 3 days. Further procedure was similar for all immunofluorescent staining experiments. The scaffolds were fixed using a 4% paraformaldehyde solution (Sigma-Aldrich, UK) for 15 min. Following fixation, the samples were washed with PBS and then incubated in a 0.1% Triton X-

100 solution (Sigma-Aldrich, UK) for 10 min, followed by rinsing with PBS. To prevent nonspecific binding, a blocking step was performed by incubating the samples in a 3% bovine serum albumin (BSA, Sigma-Aldrich, UK) solution in PBS for 60 min. Monoclonal anti-paxillin antibodies (ab32084, Abcam, UK) were used to stain the focal adhesion complex, and the samples were incubated with these antibodies overnight. After staining, the samples were rinsed with PBS for 15 min. Subsequently, the cells were incubated with an anti-rabbit secondary antibody conjugated with Alexa Fluor Plus 555 (A32732, Thermo Fisher, USA) for 1 h. To visualize actin, cells were incubated with Alexa Fluor™ 488 Phalloidin (Thermo Fisher, USA) for 1 h at 23 ºC. The last step involved nuclear staining using DAPI for 15 min.

Confocal microscopy (Zeiss LSM 900, Germany) was used to acquire the images. Different objectives, including Plan-Apochromat 10x/0.45 M27, 20x/0.8 M27, 40x/1.30 Oil DIC M27, and 63×/1.4 Oil DIC M27, were utilized during the experiments. For the excitation of DAPI, Alexa Fluor™ 488 Phalloidin, and Alexa Fluor Plus 555, laser lines at 405 nm, 488 nm, and 555 nm were used, respectively[31]. The following parameters were used for Airyscan confocal superresolution microscopy: Plan-Apochromat 63×/1.4 Oil DIC M27, excitation 488 nm, 561 nm, emission detection bands 500 – 550 nm for Alexa Fluor 488 coupled with Phalloidin, 560 – 700 nm for Alexa Fluor 555[28]. Registration was performed in sequential mode, 16-bit dynamic range.

2.8.3. SEM imaging of cells

Cells were fixed after 1, 3 and 7 days of culture with 2.5 % glutaraldehyde (Sigma-Aldrich, UK) for 1 h at 25 ºC. In the next step, samples were rinsed three times with PBS for further dehydration in ethanol solution series (Avantor, Poland) (50 %, 70 %, 80 %, 90 %, 100 %). Incubation in each ethanol solution lasted 7 min and was repeated twice for 100 % solution, followed by incubation in hexamethyldisilazane (HDMS, Sigma-Aldrich, UK) under a fume hood until complete

evaporation of HDMS. SEM imaging and Au coating of cells on scaffolds were done using the same parameters for the fiber characterization mentioned above.

3. Results and discussion

3.1. Scaffold characterization

PMMA fibers were electrospun using a single nozzle, contrary to PC-PMMA core-shell fibers produced using coaxial multichannel spinneret, schematically shown in **Figure 1 A)**. In core-shell electrospinning, a droplet emerges at the exit point of the core-shell nozzle, which takes on a shape resembling a Taylor cone due to the attractive influence of electric Maxwell stresses exerted on the liquid[32]. Within the cone, the liquid experiences an electric field, leading to the formation of a compound jet. This jet then undergoes the bending instability propelled by electrical forces, similar to the typical electrospinning process. This instability-induced stretching of the jet is accompanied by significant thinning and rapid solvent evaporation. Consequently, the core-shell jet solidifies, and the resulting core-shell fibers are deposited onto a collector[32,33]. Performed SEM of randomly electrospun PMMA and core-shell PC-PMMA fibers shows smooth, beads-free morphology, **Figure 1 B), E),** which proves obtained stable process of electrospinning[34]. The average fiber diameter (D_f) for PMMA fibers reached 2 ± 0.35 μm, while for core-shell PC-PMMA increased to 4.94 ± 0.88 μm. The histograms of fiber diameter for both samples show unimodal distribution, **Figure 1 H)**. Samples were manually stretched and imaged using SEM to observe the mechanical behaviour of materials. PMMA fibers demonstrated a brittle character, while core-shell fibers present a more elastic PC core and brittle PMMA shell damaged by mechanical deformation, **Figure 1 C), F)**. Additionally, freeze fractures were done to present proper solid PMMA fibers and core-shell PC-PMMA formation, **Figure 1 D), G)**. Contact angle

measurement led to a comparison of wetting properties of scaffolds, where for PMMA, the average contact angle was 120.94 ± 4.21 °, and for PC-PMMA, 124.75 ± 3.86 °, indicating a similar hydrophobic nature of both types of fibers. Examples of images used for measurements are presented in **SI Figure S1**. Verification of bulk chemistry was performed using FTIR and allowed to prove the existence of PC in core-shell fibers, **Figure 1 I)**. The presence of PMMA in core-shell fibers was confirmed by peaks at 2950 and 2990 cm^{-1}, observed for PMMA powder, PMMA fibers, and PC-PMMA fibers, which correspond to α-methyl, ester – methyl, and methylene C-H stretching[35]. Furthermore, for all samples consisting of PMMA was observed peak at 1728 cm^{-1} responsible for the C=O group stretching mode belonging to PMMA polymer[35,36]. Identification of PC in core-shell fibers was verified by the characteristic peak at 1768 cm^{-1} associated with the carbonyl group, present for both PC pellets and PC-PMMA fibers[37]. The thermal properties of the two types of fibers were analyzed using DSC, and results show differences in glass transition temperature (T_g), **Figure 1 J)**. PMMA fibers exhibit an average T_g = 105.29 °C, around 8 ° higher than the average T_g of PC-PMMA core-shell fibers.

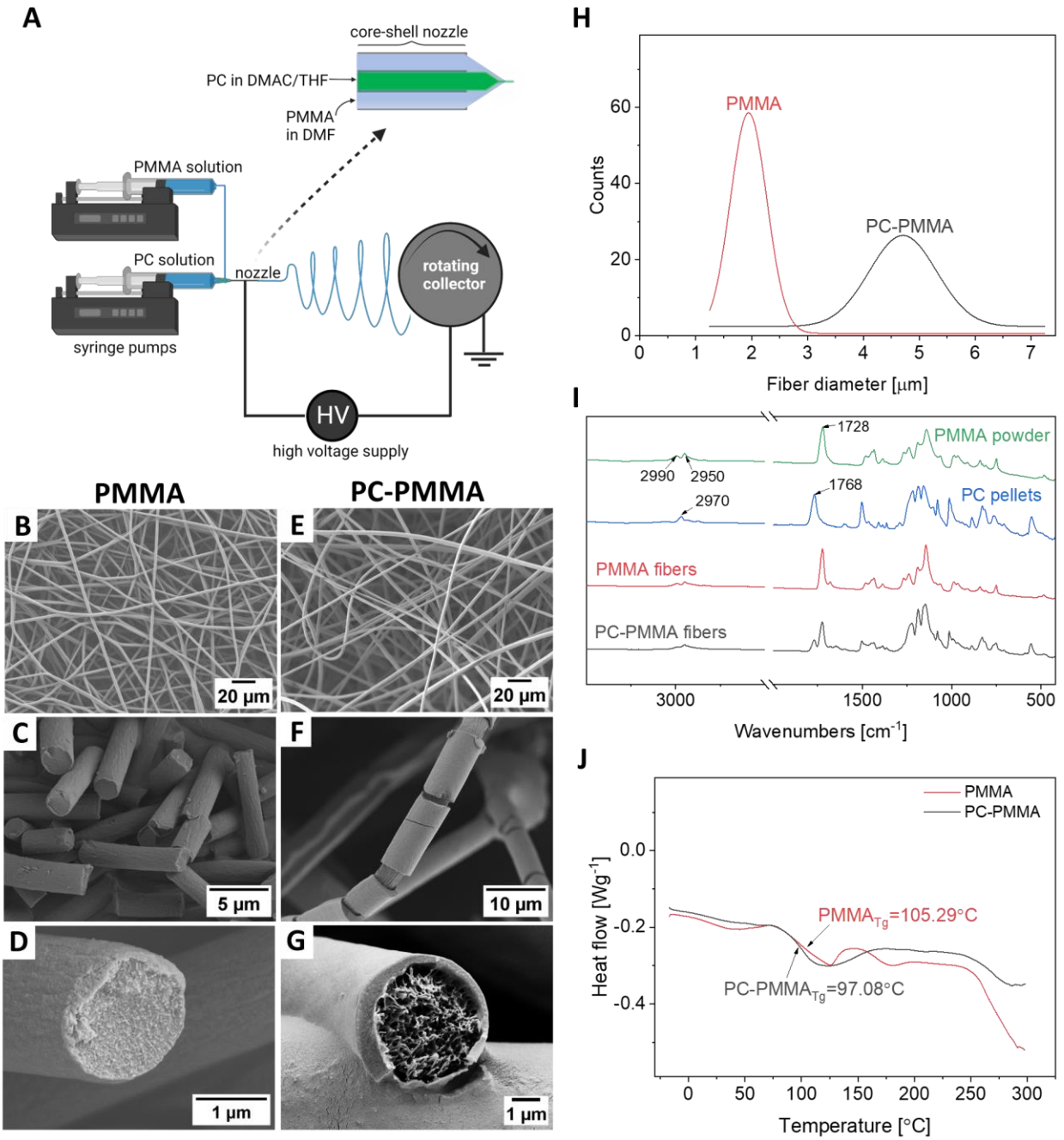

Figure 1. A) Scheme of core-shell electrospinning with a focus on the core-shell nozzle. SEM micrographs of B)-D) PMMA, and E)-G) PC-PMMA fibers. H) Fiber diameter distribution graph (Gaussian fit), I) FTIR results of PMMA powder, PC pellets, PMMA, and PC-PMMA fibers. J) DSC of PMMA and PC-PMMA scaffolds.

3.2. Mechanical testing

The distinctive mechanical behaviour of pure PMMA fibers and core-shell PC-PMMA fibers was observed after manual stretching fibrous mats and SEM imaging. It confirms the possibility of manipulating the mechanical properties of PMMA fibers via co-axial processing[38]. PMMA fibers showed brittleness in opposition to core-shell fibers in which PC core tends to elongate, while the rigid shell cracked, **Figure 1 C), F)**. This observation was verified with the mechanical testing of fibrous scaffolds. In **Figure 2 A), B),** stress–strain curves are shown after tensile testing of PMMA and PC-PMMA scaffolds. Both curves show sharp stress peaks, which are characteristic for PMMA because for both samples strain at maximum stress is similar, 1.81 ± 0.52 % for PMMA fibers, and 2.15 ± 0.46 % for PC-PMMA, see **Table 1**. PC-PMMA fibers obtained a maximum stress value of more than two times higher, as well as an elongation of 200%, which is 10 times higher compared to PMMA fibers. Moreover, the resulting toughness is 50 times higher for PC-PMMA fibers, demonstrating a significant trend of higher mechanical properties for core-shell fibrous mats which was also previously reported for aligned PMMA and PC-PMMA fibers[38].

Additionally, the tensile tests of individual PMMA and core-shell PC-PMMA fibers were performed indicating much higher maximum tensile stress and elastic modulus for PMMA fibers. This trend is similar for both single and two fibers measurements. However, the elongation at failure for core-shell PC-PMMA single fiber (**Figure 2 D)**) is more than 100 times higher compared to PMMA (**Figure 2 C)**). Furthermore, the stress-strain curves of individual PC-PMMA fibers show sharp peaks around the strain of 100 %, which can be assigned to the characteristic brittle behaviour of PMMA. The Young's modulus for PMMA is also two orders of magnitude higher for individual fibers than for core-shell PC-PMM, indicating higher stiffness of PMMA

than PC. Basically, our results confirm that PMMA is intrinsically brittle and PC is more ductile[39].

Table 1. Tensile test results for PMMA and PC-PMMA mats, single fiber and two fibers. With the characteristics values of elongation at failure (Ɛf), maximum stress (Rm), toughness (W), elongation at maximum stress (Ɛmax), and Young's Modulus €. Errors are based on standard deviation, with N = 5, where N is the tensile test of one mat sample.

Sample	$Ɛ_f$ [%]	R_m [MPa]	W [$MJ \cdot m^{-3}$]	$Ɛ_{max}$ [%]	E [MPa]
PMMA mat	19.41 ± 4.52	58.31 ± 14.24	2.25 ± 0.82	1.81 ± 0.53	
PC-PMMA mat	260.39 ± 33.09	142.89 ± 51.64	117.71 ± 29.91	2.15 ± 0.46	
PMMA 1 fiber	8.9	128.03	9.2	8.5	58.20 ± 7.98
PMMA 2 fibers	15.4	537.26	62.92	12.2	98.83 ± 4.31
PC-PMMA 1 fiber	1003.7	6.53	40.21	341.2	0.51 ± 0.27
PC-PMMA 2 fibers	1012.9	18.84	108.11	117.2	0.61 ± 0.17

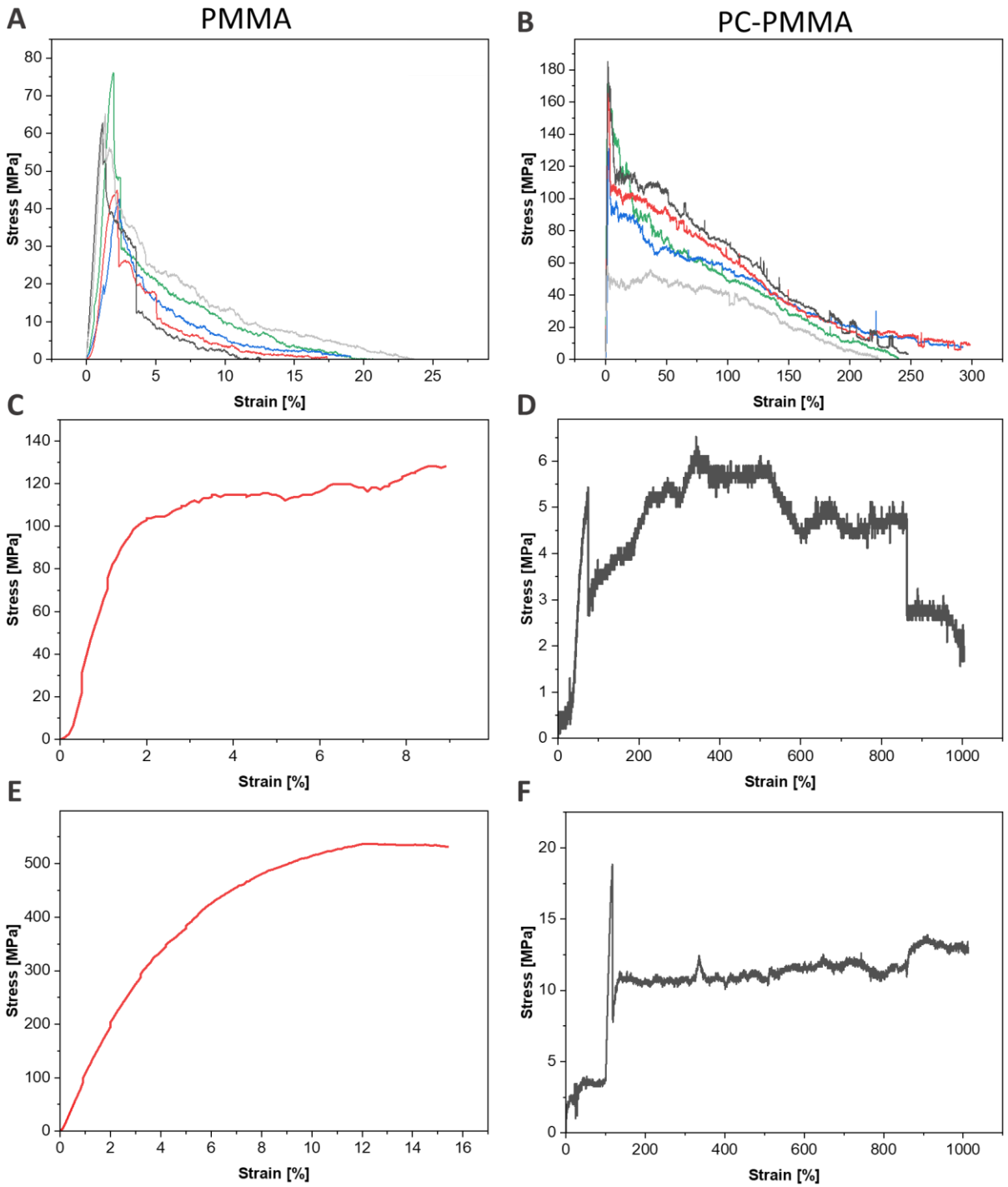

300

301 **Figure 2.** Stress-strain curves of A) PMMA and B) PC-PMMA mats; C) PMMA and D) PC-

302 PMMA single fibers; E) PMMA and F) PC-PMMA two fibers.

303

3.3. Surface properties of scaffolds

The differences in the surface chemistry investigated via XPS analysis of PMMA fibers and PC-PMMA core-shell fibers are caused by diffusion of core material toward fiber surface, which is schematically shown in **Figure 3 A)**. Identification of PC in the surface of the core-shell fibers using XPS showed the presence of carbonate group (-O-(C=O)-O-) in our electrospun fibers. XPS spectra of PMMA and PC-PMMA from the measurement depth of 1.4 nm are shown in **Figure 3 B), C)**. Additionally, all the XPS spectra obtained at depths of 1.4 and 8 nm, performed at different measurement angles, are included in **Supplementary Information, Figure S2**. We observed increased intensity of peak energy at 289 eV, characterizing the O-C=O group present in PMMA. Carbon from this group marked as C4 in **Figure 3 D)** and **Table 2**, is present in both PMMA and PC-PMMA fibers, regardless of measurement depth. Carbon from the carbonate group of PC found at a binding energy of 291 eV (C5 in **Figure 3 D**) and **Table 2**) was present in PC-PMMA fibers in both 1.4 and 8 nm depth of measurement in similar concentrations, proving diffusion of PC from the core to the surface of the fiber, see **Table 2**. Herein, we assume that interdiffusion between two miscible solutions was possible before the ejection of the compound jet, which occurred as the two solutions first met in the cone formed at the end of the coaxial nozzle[40,41]. Moreover, it was reported that this interdiffusion during the co-electrospinning process can lead to partial or complete mixing of core and shell layers[41–43]. Further, as the surface chemistry of our core-shell fibers is not pure PMMA, we performed additional surface analysis related to the surface potential of electrospun fibers used as scaffolds in tissue engineering. Charges at the surface of polymer fibers can be controlled by electrospinning parameters, especially via applied voltage polarity[44,45] It has a significant effect on the surface free energy of polymers[46,47], and their triboelectric performance[48] and follows with the cell interactions once placed in cell culture

studies[3,49]. Higher surface potential can improve the adhesion of cells to fibers; thus, this effect should also be considered in later cell culture studies [50–53]. Therefore, in **Figure 3 E)** we present KPFM maps of fibers topography and surface potential. Measurements show around 150 mV higher surface potential of PMMA fibers, where the values were ~650 mV for PMMA, and ~500 mV for PC-PMMA fibers, see **Figure 3 F)**.

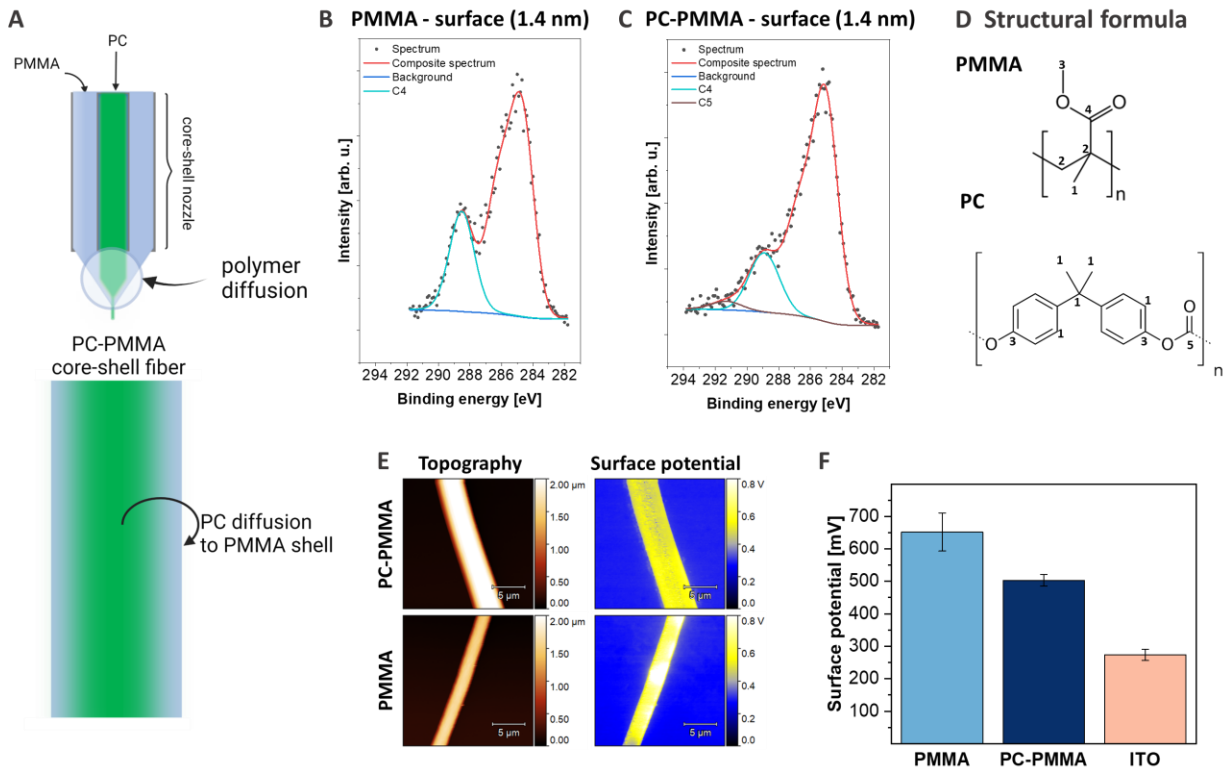

Figure 3. A) Scheme of core polymer diffusion in core-shell fiber. XPS spectra of B) PMMA, and C) PC-PMMA. D) Structural formula of PMMA and PC. E) KPFM maps of fibers topography and surface potential, and F) calculated values of surface potential (error bars present standard deviation calculated for N = 7, where N is the surface potential value for one fiber scan or scan of the ITO reference).

Table 2. XPS results for PMMA and PC-PMMA samples at two angles, 10 and 90 °, corresponding to 1.4 and 8 nm measurement depth, respectively. The full spectra are presented in **SI, Figure S2**.

Measurement depth [nm]	PMMA				PC-PMMA				
	C1	C2	C3	C4	C1	C2	C3	C4	C5
	[%]				[%]				
1.4	25.9	14.3	14.2	18.8	36.9	11.2	16.1	13.7	2.2
8	26.6	16.8	15.3	14.2	40.1	12.3	14.2	9.4	2.0

3.4. Cellular behaviour to material properties

3.4.1. Cell proliferation

The proliferation assay, see **Figure 4 A)**, was performed to analyze the viability of cells on polymer scaffolds after 1, 3 and 7 days of culture. Results for both samples show a continuously increased number of osteoblasts with cell culture time. However, a significant difference in proliferation between the samples was observed after 7 days, indicating 28 % better viability of cells on PMMA fibers. In the standard confocal microscopy, we used a low-magnification lens with a large depth of field, as presented in the scheme in **Figure 4 B)**, which gave us the ability to image cells on scaffolds and obtain comparable information about cell morphology as from SEM micrographs. As a control, cells were seeded and cultured on glass and further imaged with the confocal microscope, see **SI, Figure S3**. Notably, the proliferation results are consistent with the recorded SEM and CLSM images. Higher proliferation was observed on PMMA fibers after 7 days of cell culture, clearly visible contrasting PMMA scaffold after day 7, **Figure 4 H)**, and PC-PMMA sample, **Figure 4 N)**. Studies show that increased replicative activity of immortalized cell

lines is observed only after 3 and even after 5 days of incubation. Hence, differentiated cell proliferation in response to the properties of electrospun fibers are observed after this time[4]. The further examination indicates that cells on the PMMA fibers tend to create solid and dense structures, which is a different behaviour than on PC-PMMA fibers, where cells were more distributed and less numerous. Additionally, cells on core-shell fibers were stretched more with longer filopodia. These morphological differences can be caused by different mechanical properties of fibers or surface properties like surface potential, higher for PMMA fibers which can promote better proliferation and adhesion of cells[53]. Generally, the diameter of fibers constructing scaffolds influences cell morphology[4,54]; however, PMMA and PC-PMMA fiber diameters are in the same order of magnitude. It was already reported that PCL electrospun scaffolds with a fiber diameter range of 1µm to 8 µm did not affect the proliferation of stem cells[55]. Consequently, this aspect was neglected. In the context of tissue engineering, the mechanical properties of scaffolds play a vital role at the cellular scale related to mechanotransduction. It pertains to the intricate molecular pathways through which cells perceive external forces and exert forces onto a substrate[56,57]. Throughout all stages of tissue development, cells, ranging from stem cells to mature cells, possess mechanoreceptors on their cell surface, enabling them to perceive their mechanical surroundings. Upon initial contact with the extracellular matrix, integrins, which are adhesive molecules on the cell surface, bind with ligands present on the matrix surface. This interaction leads to the formation of significant protein complexes known as focal adhesions, which anchor the cell cytoskeleton to the matrix. These intricate nanoscale processes are crucial in determining the cell's attachment points, morphology, and, ultimately, their function[58]. While core-shell fibers hold the potential for independently regulating cell-matrix mechanical interaction regardless of surface chemistry, none of the studies

have conducted measurements of the micromechanics of these fibers at the cell-sensing scale[14,59]. Furthermore, we show the inseparable impact of core material on surface potential and surface chemistry, which strongly affects cellular responses[50,53,60].

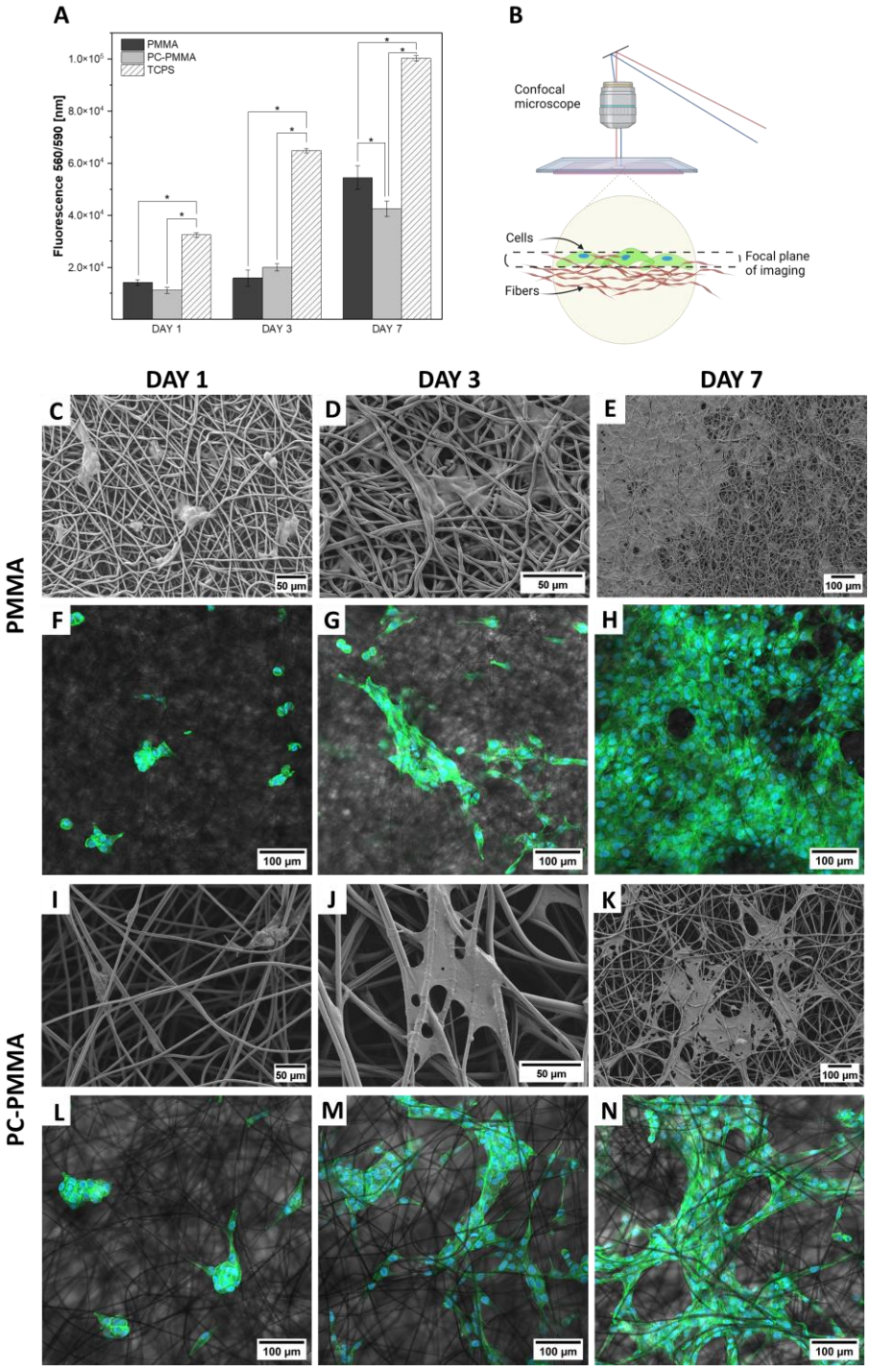

Figure 4. Results from cell culture studies showing A) proliferation assay of osteoblasts on PMMA and PC-PMMA scaffolds. B) Scheme of the focal plane of imaging in confocal microscope investigation of scaffolds. SEM micrographs of cell culture after 1, 3, and 7 days on C) – E) PMMA, and F) – H) PC-PMMA scaffolds with corresponding CLSM images of F) – H) PMMA and L) – N) PC-PMMA scaffolds. Actin (green) stained with Alexa Fluor™ 488 Phalloidin and nuclei (blue) with DAPI. *Statistical significance is calculated with ANOVA, followed by Tukey's post-hock test, $p < 0.05$; error bars are based on standard deviation.

3.4.2. Morphology and focal adhesion analysis

To investigate cell morphology and adhesion, single fibers of the analyzed samples were deposited on glass, and in the next step, cells were seeded and incubated for 3 days. After actin and paxillin were stained, confocal microscopy imaging was performed. This approach allowed us to obtain information about cell adhesion to glass and fiber from the same focal plane. The imaging parameters were identical regardless of the type of adhesion and the type of sample, which makes it possible to correlate the intensity of the signal with the amount of protein molecules accumulating at the cell-material contact sites. Actin provides insight into the cell's morphology and shape, whereas paxillin functions as one of the focal adhesion proteins. Focal adhesions are complex structures containing integrins and multiple proteins, which create mechanical connections between the intracellular actin bundles and the extracellular substrate in various cell types. These focal adhesions are sizeable and dynamic protein complexes consisting, among other proteins, of paxillin, vinculin, talin, or zyxin that enable the cell's cytoskeleton to link with the ECM[61,62]. Here, we use paxillin as an immunofluorescent marker to label the distribution of cell adhesion sites. For imaging the focal adhesion sides localization, the Airyscan confocal

409 superresolution method was used[28]. For both samples, cells created advanced actin structure,
410 which confirms accurate morphology, see **Figure 5 C), G)**. Focal adhesions of osteoblasts to glass
411 for PMMA (**SI Figure S4 I), II), III)**) as well as PC-PMMA (**SI Figure S4 IV), V), VI)**) samples
412 show characteristic patterns and similar intensity compared to each other[62]. Interestingly, we
413 observed completely different adhesion of cells to PMMA and PC-PMMA fibers. Adhesion to
414 PMMA is intensive, and the amount of proteins is enormous (**Figure 5 I, II, III**), while adhesion
415 to PC-PMMA fiber is hardly seen (**Figure 5 IV, V, VI**). For more precise results in the difference
416 in focal adhesion to both types of fibers, we analyzed signal intensity profiles based on Airyscan
417 images.

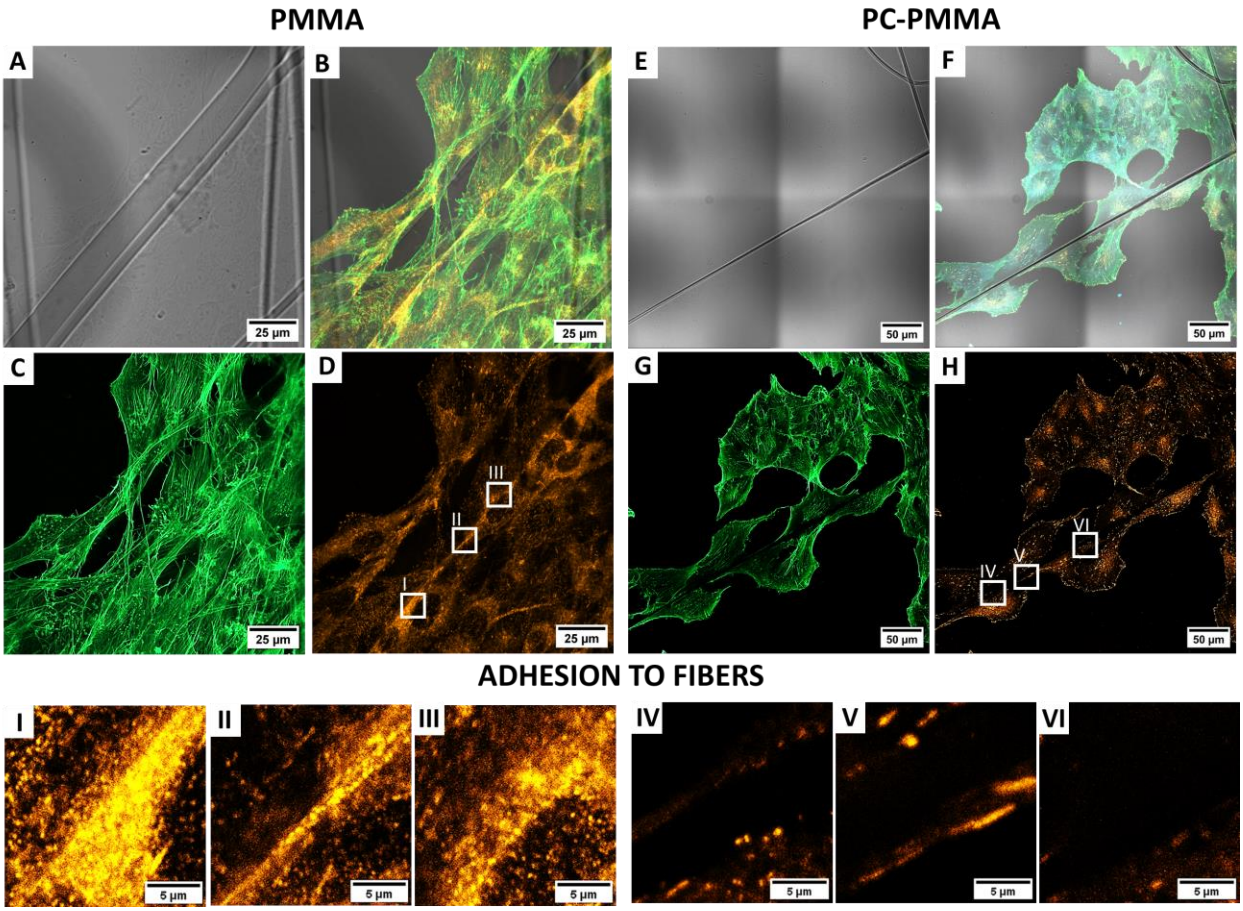

418

419 **Figure 5.** Focal adhesions analysis on PMMA fibers: A) in transmitted light channel, B) merged
420 channels, C) stained actin (green), D) stained paxillin (orange). Zoom on paxillin from the cell

adhesion to PMMA fiber images I) – III). Focal adhesions analysis on PC-PMMA fibers: E) in transmitted light channel, F) merged channels, G) stained actin (green), H) stained paxillin (orange). Zoom on paxillin from the cell adhesion to PC-PMMA fiber images IV) – VI). Paxillin and actin stained with Alexa Fluor™ Plus 555, Alexa Fluor™ 488 Phalloidin, respectively.

To analyze the intensity of the signal coming from paxillin, actin filaments, which allow detection of the cell body, were also stained, see **Figure 6 A), C)**. The cells show stretching along the fiber for both samples. Areas of paxillin in contact between the cell and the fiber were determined from which signal intensity analysis was performed for PMMA (**Figure 6 B)**) and for PC-PMMA sample (**Figure 6 D)**). Despite the difference in paxillin distribution and signal intensity being confirmed, paxillin in PC-PMMA sample does not form as numerous adhesion sites as when interacting with PMMA. Local accumulation foci are very few, **Figure 6 D)**. The signal intensity of focal points is about 7-8 times lower (**Figure 6 G), H)**) than for paxillin at sites of adhesion to PMMA (**Figure 6 E), F)**). This indicates that the number of paxillin molecules involved in the adhesion process to PC-PMMA fibers is many times lower, making the strength and efficiency of adhesion to PC-PMMA fibers much lower. Weaker cell adhesion to PC-PMMA fibers correlates with inferior proliferation on PC-PMMA scaffolds compared to PMMA. While PMMA is a well-studied polymer with high biocompatibility tested on osteoblast cell cultures[63,64], we assume that diffused PC in core-shell fibers is responsible for decreased proliferation and adhesion due to the possible presence of residual xenohormone Bisphenol A (BPA)[65]. This study indicates that even infinitesimal diffusion of core polymer toward the surface of the core-shell fiber alters a number of fiber surface property parameters conditioning cell behaviour and, in this particular example, lowers the biocompatibility of PMMA shell.

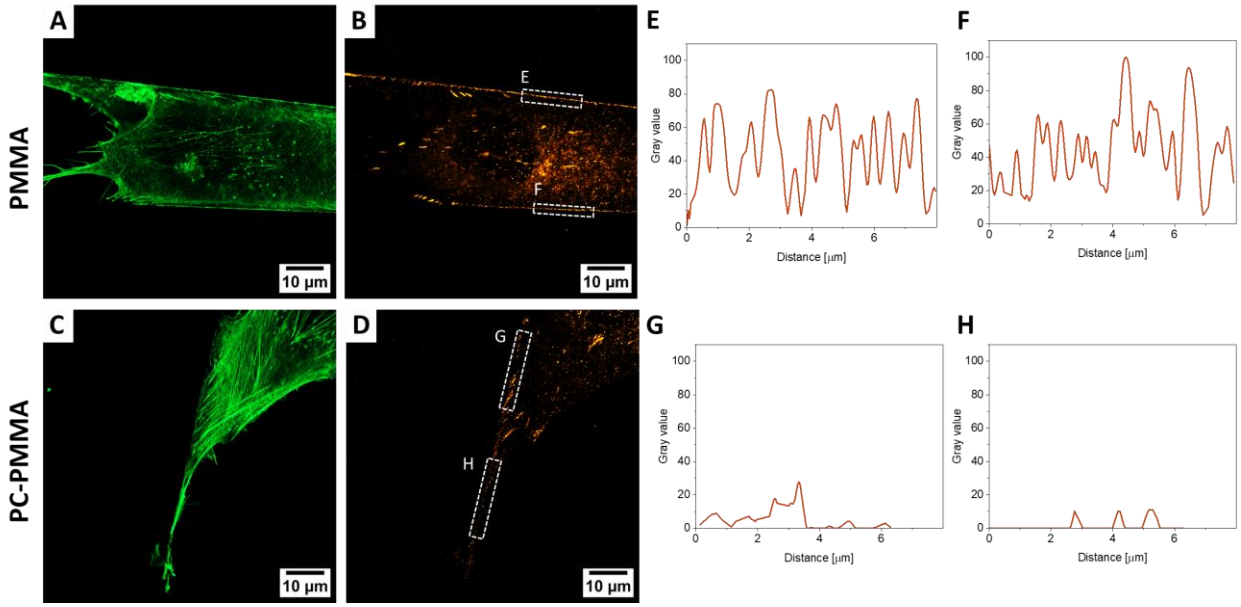

Figure 6. Airyscan images of stained actin (green) A) and paxillin (orange) B) for PMMA sample with signal intensity profiles of paxillin from marked regions E), F). Analogously, images of stained actin (green) C) and paxillin (orange) D) for PC-PMMA sample with signal intensity profiles of paxillin from marked regions G), H).

4. Conclusions

Co-axial electrospinning is a challenging process used to produce core-shell fibers combining properties of two different materials. It is possible to provide unique fiber features due to the variations in chemical composition and mechanical properties between core and shell, which is attractive in biomaterial applications. For the first time, our study shows the complexity of polymer interfacial blending occurring during co-axial electrospinning for further surface chemistry, surface potential, and mechanical properties of fibers. We conducted a cell culture study to verify if diffusion of core polymer is significant in affecting cell responses. Notably, after 7 days of cell culture, we observed 28 % higher cell viability on PMMA than on PC-PMMA fibers. Additionally,

with around 7 times stronger signal intensity, the focal adhesion point analysis indicated much stronger osteoblasts adhesion to the PMMA fibers. These favorable cellular responses to PMMA fibers were attributed to preferable surface properties, which were different in core-shell fibers because of the interfacial blending of polymers during co-axial electrospinning, resulting in the occurrence of PC in the fiber surface. The proliferation assay and the focal adhesion point analysis clearly show decreased biocompatibility of core-shell fibers caused by the diffusion of the less biocompatible core material toward the fiber surface. By using focal adhesion point analysis, we demonstrate the necessity to consider the influence of diffusion phenomena in co-axial electrospinning on the design of core-shell fiber surface properties for applications in tissue engineering or drug delivery systems.

Notes

The authors declare that they have no known competing financial interests or personal relationships that could have appeared to influence the work reported in this paper. The raw/processed data required to reproduce this finding are available on request.

ACKNOWLEDGMENT

This study was conducted with funding from the OPUS 17 project grant provided by the National Science Centre in Poland. No 2019/33/B/ST5/01311. The confocal microscopy studies were supported by the project “Nanofiber-based sponges for atopic skin treatment” carried out within the First TEAM program of the Foundation for Polish Science co-financed by the European Union under the European Regional Development Fund, No POIR.04.04.00-00-

4571/17-00. DSC and FTIR measurements were performed within the BioCom4SavEn project funded by the European Research Council under the European Union's Horizon 2020 Framework Programme for Research and Innovation (ERC grant agreement no. 948840).

Schemes were created using BioRender.com.

REFERENCES

[1] Z.J. Krysiak, U. Stachewicz, Urea-Based Patches with Controlled Release for Potential Atopic Dermatitis Treatment, Pharmaceutics 14 (2022) 1494. https://doi.org/10.3390/pharmaceutics14071494.

[2] S. Metwally, D.P. Ura, Z.J. Krysiak, Ł. Kaniuk, P.K. Szewczyk, U. Stachewicz, Electrospun PCL patches with controlled fiber morphology and mechanical performance for skin moisturization via long-term release of hemp oil for atopic dermatitis, Membranes (Basel) 11 (2021) 1–13. https://doi.org/10.3390/membranes11010026.

[3] Ł. Kaniuk, S. Ferraris, S. Spriano, T. Luxbacher, Z. Krysiak, K. Berniak, A. Zaszczynska, M.M. Marzec, A. Bernasik, P. Sajkiewicz, U. Stachewicz, Time-dependent effects on physicochemical and surface properties of PHBV fibers and films in relation to their interactions with fibroblasts, Appl Surf Sci 545 (2021). https://doi.org/10.1016/j.apsusc.2021.148983.

[4] Z.J. Krysiak, P.K. Szewczyk, K. Berniak, E.A. Sroczyk, E. Boratyn, U. Stachewicz, Stretchable skin hydrating PVB patches with controlled pores' size and shape for deliberate evening primrose oil spreading, transport and release, Biomaterials Advances 136 (2022). https://doi.org/10.1016/j.bioadv.2022.212786.

[5] B. Azimi, H. Maleki, L. Zavagna, J.G. de la Ossa, S. Linari, A. Lazzeri, S. Danti, Bio-based electrospun fibers for wound healing, J Funct Biomater 11 (2020). https://doi.org/10.3390/JFB11030067.

[6] J. Lin, W. Zhou, S. Han, V. Bunpetch, K. Zhao, C. Liu, Z. Yin, H. Ouyang, Cell-material interactions in tendon tissue engineering, Acta Biomater 70 (2018) 1–11. https://doi.org/10.1016/j.actbio.2018.01.012.

[7] D. Grafahrend, J.L. Calvet, K. Klinkhammer, J. Salber, P.D. Dalton, M. Möller, D. Klee, Control of protein adsorption on functionalized electrospun fibers, Biotechnol Bioeng 101 (2008) 609–621. https://doi.org/10.1002/bit.21928.

[8] N. Su, P.L. Gao, K. Wang, J.Y. Wang, Y. Zhong, Y. Luo, Fibrous scaffolds potentiate the paracrine function of mesenchymal stem cells: A new dimension in cell-material interaction, Biomaterials 141 (2017) 74–85. https://doi.org/10.1016/j.biomaterials.2017.06.028.

[9] S. Sankar, C.S. Sharma, S.N. Rath, S. Ramakrishna, Electrospun Fibers for Recruitment and Differentiation of Stem Cells in Regenerative Medicine, Biotechnol J 12 (2017). https://doi.org/10.1002/biot.201700263.

[10] M.C. Amores de Sousa, C.A.V. Rodrigues, I.A.F. Ferreira, M.M. Diogo, R.J. Linhardt, J.M.S. Cabral, F.C. Ferreira, Functionalization of Electrospun Nanofibers and Fiber Alignment Enhance Neural Stem Cell Proliferation and Neuronal Differentiation, Front Bioeng Biotechnol 8 (2020). https://doi.org/10.3389/fbioe.2020.580135.

[11] A. Saudi, S. Amini, N. Amirpour, M. Kazemi, A. Zargar Kharazi, H. Salehi, M. Rafienia, Promoting neural cell proliferation and differentiation by incorporating lignin into electrospun poly(vinyl alcohol) and poly(glycerol sebacate) fibers, Materials Science and Engineering C 104 (2019). https://doi.org/10.1016/j.msec.2019.110005.

[12] M. Abedin, N. King, Diverse evolutionary paths to cell adhesion, Trends Cell Biol 20 (2010) 734–742. https://doi.org/10.1016/j.tcb.2010.08.002.

[13] J. Hao, C. Qin, C. Wu, Three-dimensional multicellular biomaterial platforms for biomedical application, Interdisciplinary Materials 2 (2023) 714–734. https://doi.org/10.1002/idm2.12122.

[14] K.M. Kennedy, A. Bhaw-Luximon, D. Jhurry, Cell-matrix mechanical interaction in electrospun polymeric scaffolds for tissue engineering: Implications for scaffold design and performance, Acta Biomater 50 (2017) 41–55. https://doi.org/10.1016/j.actbio.2016.12.034.

[15] J.E. Karbowniczek, D.P. Ura, U. Stachewicz, Nanoparticles distribution and agglomeration analysis in electrospun fiber based composites for desired mechanical performance of poly(3-hydroxybuty-rate-co-3-hydroxyvalerate (PHBV) scaffolds with hydroxyapatite (HA) and titanium dioxide (TiO2) towards medical applications, Compos B Eng 241 (2022) 110011. https://doi.org/10.1016/j.compositesb.2022.110011.

[16] Z.J. Krysiak, U. Stachewicz, Electrospun fibers as carriers for topical drug delivery and release in skin bandages and patches for atopic dermatitis treatment, Wiley Interdiscip Rev Nanomed Nanobiotechnol 15 (2023). https://doi.org/10.1002/wnan.1829.

[17] J. Wu, Z. Zhang, J. Gu, W. Zhou, X. Liang, G. Zhou, C.C. Han, S. Xu, Y. Liu, Mechanism of a long-term controlled drug release system based on simple blended electrospun fibers, Journal of Controlled Release 320 (2020) 337–346. https://doi.org/10.1016/j.jconrel.2020.01.020.

[18] B. Ghafoor, A. Aleem, M. Najabat Ali, M. Mir, Review of the fabrication techniques and applications of polymeric electrospun nanofibers for drug delivery systems, J Drug Deliv Sci Technol 48 (2018) 82–87. https://doi.org/10.1016/j.jddst.2018.09.005.

[19] G.R.R.-A.B.T.L.C.J. Williams, Nanofibres in Drug Delivery, UCL Press, 2018. https://doi.org/10.14324/111.9781787350182.

[20] R.A. Perez, H.W. Kim, Core-shell designed scaffolds for drug delivery and tissue engineering, Acta Biomater 21 (2015) 2–19. https://doi.org/10.1016/j.actbio.2015.03.013.

[21] J.W. Drexler, H.M. Powell, Regulation of electrospun scaffold stiffness via coaxial core diameter, Acta Biomater 7 (2011) 1133–1139. https://doi.org/10.1016/j.actbio.2010.10.025.

[22] D. Rybak, C. Rinoldi, P. Nakielski, J. Du, M.A. Haghighat Bayan, S.S. Zargarian, M. Pruchniewski, X. Li, B. Strojny-Cieslak, B. Ding, F. Pierini, Injectable and self-healable nano-architectured hydrogel for NIR-light responsive chemo- and photothermal bacterial eradication, J Mater Chem B (2024). https://doi.org/10.1039/d3tb02693k.

[23] Y. Lu, J. Huang, G. Yu, R. Cardenas, S. Wei, E.K. Wujcik, Z. Guo, Coaxial electrospun fibers: applications in drug delivery and tissue engineering, Wiley Interdiscip Rev Nanomed Nanobiotechnol 8 (2016) 654–677. https://doi.org/10.1002/wnan.1391.

[24] M.M. Kareem, T. Hodgkinson, M.S. Sanchez, M.J. Dalby, K.E. Tanner, Hybrid core-shell scaffolds for bone tissue engineering, Biomedical Materials (Bristol) 14 (2019). https://doi.org/10.1088/1748-605X/aafbf1.

[25] D. Ji, Y. Lin, X. Guo, B. Ramasubramanian, R. Wang, N. Radacsi, R. Jose, X. Qin, S. Ramakrishna, Electrospinning of nanofibres, Nature Reviews Methods Primers 4 (2024). https://doi.org/10.1038/s43586-023-00278-z.

[26] J.E. Karbowniczek, K. Berniak, J. Knapczyk-Korczak, G. Williams, J.A. Bryant, N.D. Nikoi, M. Banzhaf, F. de Cogan, U. Stachewicz, Strategies of nanoparticles integration in polymer fibers to achieve antibacterial effect and enhance cell proliferation with collagen production in tissue engineering scaffolds, J Colloid Interface Sci 650 (2023) 1371–1381. https://doi.org/10.1016/j.jcis.2023.07.066.

[27] L.E. Sperling, K.P. Reis, P. Pranke, J.H. Wendorff, Advantages and challenges offered by biofunctional core-shell fiber systems for tissue engineering and drug delivery, Drug Discov Today 21 (2016) 1243–1256. https://doi.org/10.1016/j.drudis.2016.04.024.

[28] K. Berniak, D.P. Ura, A. Piórkowski, U. Stachewicz, Cell–Material Interplay in Focal Adhesion Points, ACS Appl Mater Interfaces (2024). https://doi.org/10.1021/acsami.3c19035.

[29] S. Fusco, V. Panzetta, V. Embrione, P.A. Netti, Crosstalk between focal adhesions and material mechanical properties governs cell mechanics and functions, Acta Biomater 23 (2015) 63–71. https://doi.org/10.1016/j.actbio.2015.05.008.

[30] B. Wehrle-Haller, Structure and function of focal adhesions, Curr Opin Cell Biol 24 (2012) 116–124. https://doi.org/10.1016/j.ceb.2011.11.001.

[31] Ł. Kaniuk, K. Berniak, A. Lichawska-Cieślar, J. Jura, J.E. Karbowniczek, U. Stachewicz, Accelerated wound closure rate by hyaluronic acid release from coated PHBV electrospun fiber scaffolds, J Drug Deliv Sci Technol 77 (2022). https://doi.org/10.1016/j.jddst.2022.103855.

[32] Z. Sun, E. Zussman, A.L. Yarin, J.H. Wendorff, A. Greiner, Compound Core-Shell Polymer Nanofibers by Co-Electrospinning, Advanced Materials 15 (2003) 1929–1932. https://doi.org/10.1002/adma.200305136.

[33] A.L. Yarin, Coaxial electrospinning and emulsion electrospinning of core-shell fibers, Polym Adv Technol 22 (2011) 310–317. https://doi.org/10.1002/pat.1781.

[34] S. De Vrieze, P. Westbroek, T. Van Camp, K. De Clerck, Solvent system for steady state electrospinning of polyamide 6.6, J Appl Polym Sci 115 (2010) 837–842. https://doi.org/10.1002/app.30331.

[35] S. Sain, D. Ray, A. Mukhopadhyay, S. Sengupta, T. Kar, C.J. Ennis, P.K.S.M. Rahman, Synthesis and characterization of PMMA-cellulose nanocomposites by in situ polymerization technique, J Appl Polym Sci 126 (2012). https://doi.org/10.1002/app.36723.

[36] F.J. Tommasinia, L. da Cunha Ferreira, L.G.P. Tienne, V. de Oliveira Aguiar, M.H.P. da Silva, L.F. da Mota Rocha, M. de Fátima Vieira Marques, Poly (methyl methacrylate)-Sic nanocomposites prepared through in situ polymerization, Materials Research 21 (2018). https://doi.org/10.1590/1980-5373-mr-2018-0086.

[37] P.M. Gore, P. Gawali, M. Naebe, X. Wang, B. Kandasubramanian, Polycarbonate and activated charcoal-engineered electrospun nanofibers for selective recovery of oil/solvent from oily wastewater, SN Appl Sci 2 (2020). https://doi.org/10.1007/s42452-020-03609-x.

[38] D.P. Ura, K. Berniak, U. Stachewicz, Critical length reinforcement in core-shell electrospun fibers using composite strategies, Compos Sci Technol 211 (2021). https://doi.org/10.1016/j.compscitech.2021.108867.

[39] Z. Tang, K. Fujimoto, S. Okazaki, A comparison of the brittle PMMA with the ductile PC on the elasticity and yielding from a molecular dynamics perspective, Polymer (Guildf) 226 (2021). https://doi.org/10.1016/j.polymer.2021.123809.

[40] K. Yan, Y. Le, H. Mengen, L. Zhongbo, H. Zhulin, Effect of solution miscibility on the morphology of coaxial electrospun cellulose acetate nanofibers, Polymers (Basel) 13 (2021). https://doi.org/10.3390/polym13244419.

[41] J.T. McCann, D. Li, Y. Xia, Electrospinning of nanofibers with core-sheath, hollow, or porous structures, J Mater Chem 15 (2005) 735–738. https://doi.org/10.1039/b415094e.

[42] D. Li, Y. Xia, Direct fabrication of composite and ceramic hollow nanofibers by electrospinning, Nano Lett 4 (2004) 933–938. https://doi.org/10.1021/nl049590f.

[43] Z. Kurban, A. Lovell, S.M. Bennington, D.W.K. Jenkins, K.R. Ryan, M.O. Jones, N.T. Skipper, W.I.F. David, A solution selection model for coaxial electrospinning and its application to nanostructured hydrogen storage materials, Journal of Physical Chemistry C 114 (2010) 21201–21213. https://doi.org/10.1021/jp107871v.

[44] D.P. Ura, U. Stachewicz, The Significance of Electrical Polarity in Electrospinning: A Nanoscale Approach for the Enhancement of the Polymer Fibers' Properties, Macromol Mater Eng 307 (2022). https://doi.org/10.1002/mame.202100843.

[45] D.P. Ura, J. Knapczyk-Korczak, P.K. Szewczyk, E.A. Sroczyk, T. Busolo, M.M. Marzec, A. Bernasik, S. Kar-Narayan, U. Stachewicz, Surface Potential Driven Water Harvesting from Fog, ACS Nano 15 (2021) 8848–8859. https://doi.org/10.1021/acsnano.1c01437.

[46] U. Stachewicz, A.H. Barber, Enhanced wetting behavior at electrospun polyamide nanofiber surfaces, Langmuir 27 (2011) 3024–3029. https://doi.org/10.1021/la1046645.

[47] U. Stachewicz, C.A. Stone, C.R. Willis, A.H. Barber, Charge assisted tailoring of chemical functionality at electrospun nanofiber surfaces, J Mater Chem 22 (2012) 22935–22941. https://doi.org/10.1039/c2jm33807f.

[48] T. Busolo, D.P. Ura, S.K. Kim, M.M. Marzec, A. Bernasik, U. Stachewicz, S. Kar-Narayan, Surface potential tailoring of PMMA fibers by electrospinning for enhanced triboelectric performance, Nano Energy 57 (2019) 500–506. https://doi.org/10.1016/j.nanoen.2018.12.037.

[49] P.K. Szewczyk, K. Berniak, J. Knapczyk-Korczak, J.E. Karbowniczek, M.M. Marzec, A. Bernasik, U. Stachewicz, Mimicking natural electrical environment with cellulose acetate scaffolds enhances collagen formation of osteoblasts, Nanoscale 15 (2023) 6890–6900. https://doi.org/10.1039/d3nr00014a.

[50] S. Metwally, J.E. Karbowniczek, P.K. Szewczyk, M.M. Marzec, A. Gruszczyński, A. Bernasik, U. Stachewicz, Single-Step Approach to Tailor Surface Chemistry and Potential on Electrospun PCL Fibers for Tissue Engineering Application, Adv Mater Interfaces 6 (2019). https://doi.org/10.1002/admi.201801211.

[51] P.K. Szewczyk, S. Metwally, J.E. Karbowniczek, M.M. Marzec, E. Stodolak-Zych, A. Gruszczyński, A. Bernasik, U. Stachewicz, Surface-Potential-Controlled Cell Proliferation and Collagen Mineralization on Electrospun Polyvinylidene Fluoride (PVDF) Fiber Scaffolds for Bone Regeneration, ACS Biomater Sci Eng 5 (2019) 582–593. https://doi.org/10.1021/acsbiomaterials.8b01108.

[52] S. Metwally, S. Ferraris, S. Spriano, Z.J. Krysiak, Ł. Kaniuk, M.M. Marzec, S.K. Kim, P.K. Szewczyk, A. Gruszczyński, M. Wytrwal-Sarna, J.E. Karbowniczek, A. Bernasik, S. Kar-Narayan, U. Stachewicz, Surface potential and roughness controlled cell adhesion and collagen formation in electrospun PCL fibers for bone regeneration, Mater Des 194 (2020). https://doi.org/10.1016/j.matdes.2020.108915.

[53] M. Polak, K. Berniak, P.K. Szewczyk, J.E. Karbowniczek, M.M. Marzec, U. Stachewicz, PLLA scaffolds with controlled surface potential and piezoelectricity for enhancing cell adhesion in tissue engineering, Appl Surf Sci 621 (2023). https://doi.org/10.1016/j.apsusc.2023.156835.

[54] D.P. Ura, J.E. Karbowniczek, P.K. Szewczyk, S. Metwally, M. Kopyściański, U. Stachewicz, Cell Integration with Electrospun PMMA Nanofibers, Microfibers, Ribbons, and Films: A Microscopy Study, Bioengineering 6 (2019) 41. https://doi.org/10.3390/bioengineering6020041.

669 [55] Z. Gu, S. Fan, S.C. Kundu, X. Yao, Y. Zhang, Fiber diameters and parallel patterns:
670 Proliferation and osteogenesis of stem cells, Regen Biomater 10 (2023).
671 https://doi.org/10.1093/rb/rbad001.

672 [56] T. Mammoto, A. Mammoto, D.E. Ingber, Mechanobiology and developmental control,
673 Annu Rev Cell Dev Biol 29 (2013) 27–61. https://doi.org/10.1146/annurev-cellbio-101512-
674 122340.

675 [57] E.K. Paluch, C.M. Nelson, N. Biais, B. Fabry, J. Moeller, B.L. Pruitt, C. Wollnik, G.
676 Kudryasheva, F. Rehfeldt, W. Federle, Mechanotransduction: Use the force(s), BMC Biol
677 13 (2015). https://doi.org/10.1186/s12915-015-0150-4.

678 [58] A. Van der Flier, A. Sonnenberg, Function and interactions of integrins, Cell Tissue Res
679 305 (2001) 285–298. https://doi.org/10.1007/s004410100417.

680 [59] M.A. Haghighat Bayan, Y.J. Dias, C. Rinoldi, P. Nakielski, D. Rybak, Y.B. Truong, A.L.
681 Yarin, F. Pierini, Near-infrared light activated core-shell electrospun nanofibers decorated
682 with photoactive plasmonic nanoparticles for on-demand smart drug delivery applications,
683 Journal of Polymer Science 61 (2023) 521–533. https://doi.org/10.1002/pol.20220747.

684 [60] S. Metwally, U. Stachewicz, Surface potential and charges impact on cell responses on
685 biomaterials interfaces for medical applications, Materials Science and Engineering C 104
686 (2019). https://doi.org/10.1016/j.msec.2019.109883.

687 [61] B. Geiger, J.P. Spatz, A.D. Bershadsky, Environmental sensing through focal adhesions,
688 Nat Rev Mol Cell Biol 10 (2009) 21–33. https://doi.org/10.1038/nrm2593.

689 [62] P. Kanchanawong, G. Shtengel, A.M. Pasapera, E.B. Ramko, M.W. Davidson, H.F. Hess,
690 C.M. Waterman, Nanoscale architecture of integrin-based cell adhesions, Nature 468 (2010)
691 580–584. https://doi.org/10.1038/nature09621.

692 [63] P. Torricelli, M. Fini, G. Giavaresi, R. Botter, D. Beruto, R. Giardino, Biomimetic PMMA-
693 based bone substitutes: A comparative in vitro evaluation of the effects of pulsed
694 electromagnetic field exposure, J Biomed Mater Res A 64 (2003) 182–188.
695 https://doi.org/10.1002/jbm.a.10372.

696 [64] M. Jäger, A. Wilke, Comprehensive biocompatibility testing of a new PMMA-HA bone
697 cement versus conventional PMMA cement in vitro, J Biomater Sci Polym Ed 14 (2003)
698 1283–1298. https://doi.org/10.1163/156856203322553491.

699 [65] P. Wei, G.A. Bhat, D.J. Darensbourg, Enabling New Approaches: Recent Advances in
700 Processing Aliphatic Polycarbonate-Based Materials, Angewandte Chemie - International
701 Edition (2023). https://doi.org/10.1002/anie.202307507.

702

703